Ultrasonics Sonochemistry 102 (2024) 106728

Contents lists available at ScienceDirect

Ultrasonics Sonochemistry

journal homepage: www.elsevier.com/locate/ultson

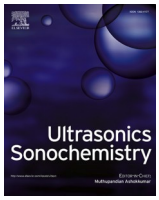

The relationship between surface drug distribution of Dox-loaded microbubbles and drug release/cavitation behaviors with ultrasound

Chia-Wei Lin [a], Ching-Hsiang Fan [b,c], Chih-Kuang Yeh [a,*]

[a] Department of Biomedical Engineering and Environmental Sciences, National Tsing Hua University, Hsinchu, Taiwan
[b] Department of Biomedical Engineering, National Cheng Kung University, Tainan, Taiwan
[c] Medical Device Innovation Center, National Cheng Kung University, Tainan, Taiwan

ARTICLE INFO

Keywords:
Doxorubicin
Fragment species
Drug release
Drug delivery
Column chromatography

ABSTRACT

Ultrasound (US)-triggered microbubbles (MBs) drug delivery is a promising tool for noninvasive and localized therapy. Several studies have shown the potential of drug-loaded MBs to boost the delivery of therapeutic substances to target tissue effectively. Nevertheless, little is known about the surface payload distribution affecting the cavitation activity and drug release behavior of the drug-loaded MBs. In this study, we designed a common chemodrug (Doxorubicin, Dox)-loaded MB (Dox-MBs) and regulated the payload distribution as uniform or cluster onto the outer surface of MBs. The Dox distribution on the MB shells was assessed by confocal fluorescence microscopic imaging. The acoustic properties of the Dox-MBs with different Dox distributions were evaluated by their acoustic stability and cavitation activities. The payload release and the fragments from Dox-MBs in response to different US parameters were measured and visualized by column chromatography and cryo-electron microscopy, respectively. By amalgamating these methodologies, we found that stable cavitation was sufficient for triggering uniform-loaded MBs to release their payload, but stable cavitation and inertial cavitation were required for cluster-loaded MBs. The released substances included free Dox and Dox-containing micelle/liposome; their portions depended on the payload distribution, acoustic pressure, cycle number, and sonication duration. Furthermore, we also revealed that the Dox-containing micelle/liposome in cluster-loaded MBs had the potential for multiple drug releases upon US sonication. This study compared uniform-loaded MBs and cluster-loaded MBs to enhance our comprehension of drug-loaded MBs mediated drug delivery.

1. Introduction

Precise, noninvasive, on-demand, and imaging-monitorable drug delivery is highly desired for tumor treatment. A recent breakthrough in this regard has emerged with the utilization of drug-loaded microbubbles (MBs) with ultrasound (US)-triggered drug delivery, offering a promising solution to address this critical unmet need. This approach uniquely combines the benefits of diagnostic imaging with the capability to target drug delivery remotely. Within an ultrasonic field, the drug-loaded MBs undergo volumetric oscillations known as cavitation, which result in the permeabilization of cellular membranes in adjacent cells, thereby enhancing drug delivery. Moreover, cavitation serves as a trigger for the controlled release of drug payloads from these microbubbles in response to US sonication. It is essential to acknowledge that most reported studies have indicated that the composition of the payload significantly influences the acoustic properties of drug-loaded MBs onto the shell of the MBs [1,2]. Leveraging these distinctive acoustic properties and drug release behaviors associated with drug-loaded MBs containing various types of surface drug distribution holds the potential to enable precise control over their behavior, thus expanding their utility in the realm of medical applications.

An increasing number of researchers have explored the potential of MBs as carriers for a wide range of therapeutic agents, including low molecular weight drugs, nanoparticles, and nucleic acids [3–6]. However, this study focuses on incorporating doxorubicin (Dox), a chemotherapy drug with known severe cardiotoxicity, as the payload for MB shell. Integrating Dox into MBs, along with US excitation, offers the prospect of significantly reducing the associated side effects of Dox, thereby enhancing its therapeutic efficacy. In our previous study, we successfully developed a novel MB formulation that permits the direct

* Corresponding author at: Department of Biomedical Engineering and Environmental Sciences, National Tsing Hua University, No. 101, Section 2, Kuang-Fu Road, Hsinchu 30013, Taiwan.
E-mail address: ckyeh@mx.nthu.edu.tw (C.-K. Yeh).

https://doi.org/10.1016/j.ultsonch.2023.106728
Received 14 October 2023; Received in revised form 23 November 2023; Accepted 12 December 2023
Available online 14 December 2023

loading of Dox onto MBs through precise modulation of the lipid components within the MB shell, obviating the need for further modifications to the Dox molecule itself [2]. While it is possible to increase the Dox payload, limited information is available regarding the relationship between the Dox payload and the cavitation behavior exhibited by the MBs. Moreover, it is imperative to thoroughly characterize the release behavior of Dox from the Dox-loaded MBs before their application.

The effectiveness of drug-loaded MBs has been extensively validated through numerous *in vitro* and *in vivo* studies. It is generally assumed that when subjected to US exposure, MBs locally release their payload. Previous studies have attempted to observe the transient drug release behavior of drug-loaded MBs and could be primarily classified into two patterns: "mist release" and "vesicle release" [7,8]. Eisenbrey et al. have reported that Dox-loaded polymer MBs ruptured, resulting in drug-containing fragments within the range of 200–400 nm, possibly due to the sonic cracking of the shell [9]. Moreover, Luan et al. and Lajoinie et al. employed high-speed fluorescence imaging to study lipid-shelled MBs (without nanoparticles) under US exposure [8]. Their investigations revealed the release of MBS shell lipids from the gas core during MBS cavitation. These liberated lipids were subsequently transported away from the membrane upon which the MBs were situated, propelled by acoustic microstreaming generated around the non-spherically oscillating MBs. Similar observations were made with liposome-loaded MBs. It has been postulated that microstreaming generated around oscillating MBs enhances the mixing of released drugs through convective flow, thereby facilitating drug delivery. Recent studies by Cock et al. and Roovers et al. have shown that drug-loaded MBs can directly print nanoparticles onto cell membranes upon US sonication [10]. This phenomenon occurred exclusively when nanoparticles were physically attached to the surface of the MBs, resulting in highly localized drug delivery. Nevertheless, limited attention has been given to understanding the mechanisms underlying the drug release process and the characteristics of the released drugs, primarily due to the reliance on optical imaging in observation strategies. Hence, it remains imperative to delve into the intricacies of drug release phenomena and the role played by drug distribution on the MB shell.

The properties of the drug-loaded MBs released payload also played an essential role for enhanced cellular uptake. For instance, free drugs, like Dox, showcase a swift cellular uptake [11], whereas its liposomal counterpart, Doxil, possesses prolonged circulation attributes [12,13]. Such distinctions highlight the inherent cellular and pharmacokinetic differences between drug-containing micelle/liposome and free drugs. Furthermore, revealing the composition of the released payload from drug-loaded MBs with various acoustic parameters, such as acoustic pressure, cycle, pulse repetition interval, and duration, is necessary. These findings underscore the multifaceted interplay between drug release mechanisms and the characteristics of the resulting fragment species [14,15].

In this study, we aim to bridge the existing knowledge gap concerning the physical factors and payload attributes governing the release of drugs from drug-loaded MBs under US sonication. Specifically, we have investigated the influence of factors such as drug surface distribution, acoustic pressures (100–550 kPa), US pulse duration (10, 100, or 1000 cycles), and US sonication duration (1, 4, 10 min) on the cavitation behavior and drug release. Since MB cavitation events transpire on a nanosecond timescale, we employ real-time passive cavitation detection to provide insights into the cavitation activities of the MBs. Additionally, column chromatography and cryo-electron microscopy (cryo-EM) are utilized to assess the characteristics of the released payload and visualize their structural attributes. By amalgamating these methodologies, we understand the mechanisms governing drug release, including the impact of payload distribution, acoustic pressure, and pulse duration on this phenomenon. Furthermore, we compare uniform-loaded MBs and cluster-loaded MBs to enhance our comprehension of drug-loaded MBs mediated drug delivery.

2. Material and methods

2.1. Preparation of L/HDox-MBs

This study employed the thin film hydration method to synthesize MBs following previous publication [2], using three types of lipids: 1,2-distearoyl-*sn*-glycero-3-phosphocholine (DSPC, Avanti Polar Lipids, AL, USA), 1,2-distearoyl-*sn*-glycero-3-phospho-*rac*-glycerol sodium salt (DSPG, Avanti Polar Lipids, AL, USA), and 1,2-distearoyl-*sn*-glycero-3-phosphoethanolamine-N-[methoxy(poly(ethylene glycol))-2000] (DSPE-PEG2000, Avanti Polar Lipids, AL, USA). DSPC, DSPG, and DSPE-PEG2000 were dissolved in chloroform with a mole ratio of 42:63:2. The solvent was subsequently removed overnight to form a thin film using an evaporator (R-210, Büchi Labortechnik, AG, Switzerland). A mixture of phosphate-buffered saline (PBS) containing 0.5 wt% glycerol, the film, and Dox was then created and uniformly dispersed at 60 °C for one hour using a sonicator (Model 2510, Branson, NY, USA). The Dox was bound onto the shell of MBs by electrostatic interaction because the Dox was anionic, and the DSPG was a cationic lipid [2,16]. Two different doses of Dox were added into the MBs suspension to modulate the distribution of Dox onto MBs shell [2]: uniform (500 μg, LDox-MBs) cluster (1500 μg, HDox-MBs). The mixed solution was then degassed and filled with perfluoropropane (C_3F_8) before being stirred at 4550 rpm for 45 s to form Dox -MBs. To eliminate unloaded Dox and surplus lipids, the solution was centrifuged at 500 g for 2 min and washed with 0.5 wt% glycerol-PBS. These procedures were repeated four times.

2.2. Characteristics of L/HDox-MBs

2.2.1. Size distribution, concentration, and payload

The size distribution and concentration of LDox-MBs and HDox-MBs were measured using a coulter counter (Multisizer 3, Beckman Coulter, FL, USA). The Dox payload was quantified in Dox-MBs after disrupting their bubble structure using a sonicator (Branson 2510, Branson Ultrasonics Corp., Danbury, CT, USA). Subsequently, the solution was mixed with methanol to suspend uniformly. Finally, the Dox amount was measured at 480 nm using a spectrophotometer (Infinite® 200PRO series, Tecan, AG, Switzerland). The encapsulation rate was estimated based on the percentage of the Dox payload on L/HDox-MBs relative to the initial Dox added. The distribution of Dox onto LDox-MBs shell and HDox-MBs shell was observed using a confocal fluorescence microscope (LSM 800, Zeiss, Oberkochen, Germany) with a 60 × oil objective (Zeiss).

2.2.2. Acoustic stability

The existence of a gas core within L/HDox-MBs was assessed via ultrasonic B-mode images. The L/HDox-MBs (concentration: 5×10^7 MBs/ml) was loaded into a 2 % agarose phantom and imaged using a 7.5-MHz ultrasonic imaging system (model t3000, Terason, MA, USA) at 37 °C [2]. B-mode images were captured continuously for an hour at 10-minute intervals. They were subsequently imported into MATLAB™ software to quantify the contrast-to-noise ratios (CNRs) of the L/HDox-MBs in each image as a measure of their echogenicity. The CNRs were calculated as the sample's backscatter signal divided by the background signal (saline only). The CNR values at each time point were normalized to 0 min for comparison.

2.2.3. Threshold for stable/inertial cavitation

Cavitation of MBs is mainly divided into stable and inertial categories. In stable cavitation, MBs oscillate rhythmically within the ultrasonic field without collapsing, promoting enhanced delivery of substances and aiding drugs in effectively reaching their targeted tissues. The dose of this can be quantified by the peak intensity difference between the fundamental signal and the subharmonic signal [17]. On the other hand, inertial cavitation involves the rapid expansion and

sudden collapse of MBs, which can increase cell permeability in ultrasonically-assisted drug delivery but may also be detrimental to surrounding tissues. Its dose is calculated based on the area within the received transducer's bandwidth [18]. Finally, we adopted the passive cavitation method to measure stable and inertial cavitation threshold [2,18,19]. The Dox-MBs (concentration: 5×10^9 MBs/ml) were loaded into a cellulose tube (diameter: 200 μm). A self-made 1-MHz US transducer (25-mm diameter) was used to excite the Dox-MBs with 1000 cycles, a pulse repetition interval (PRI) of 100 ms, and an acoustic pressure of 0–550 kPa. In the meantime, the acoustic-emission signal from the Dox-MBs was received through a 0.5-MHz focused US transducer (V303, Olympus, Westborough, MA, USA). Note that the fresh Dox-MBs were supplemented for different acoustic pressures. The 1-MHz US transducer was triggered by a waveform generator (AWG 2040, Tektronix, CA, USA) and an RF power amplifier (2100L, E&I, Rochester, NY, USA). The received signals were amplified using a pulser/receiver (Model 5072PR, Panametrics-NDT, Waltham, MA, USA) and collected by an oscilloscope (LT322, LeCroy, Chestnut Ridge, NY, USA). The received signals underwent fast Fourier transformation via MATLAB^{TM} software. The spectrum's subharmonic-frequency component (0.5 F0, 0.5 MHz) was identified as the characteristic signal of stable cavitation. The stable cavitation dose was quantified by calculating the difference in signal intensity between the fundamental signal (F_0) and the subharmonic signal. On the other hand, for inertial cavitation detection, the measurement setup was the same as the stable cavitation detection, but the receiving transducer was replaced with a 5-MHz focused US transducer (V319, Olympus, Westborough, MA, USA). The inertial cavitation dose was estimated at 4.3–4.8 MHz while specifically avoiding the harmonic and ultraharmonic frequencies of the transducer.

2.3. Column chromatography separates the fragment species of L/HDox-MBs

To identify the released payload of the Dox-MBs, column chromatography was performed after Dox-MBs were sonicated by different parameters of the US. Initially, Dox-MBs (concentration: 5×10^9 MBs/ml) were added into a 96-well plate, which was subsequently sealed with a US penetrable membrane. The 1-MHz US transducer was attached to the membrane to sonicate the Dox-MBs with a US coupling gel (Fig. 1), operating at acoustic pressure of 0–550 kPa, cycle number of 100–10000, PRI of 10–1000 ms, and duration of 1–10 min. The abovementioned waveform generator and RF power amplifier triggered the ultrasonic transducer. The fragment species of Dox-MBs in the lower layer of the sample were separated using size exclusion chromatography on a Sepharose CL-4B column. The output sample was divided into free Dox and micelle/liposome, depending on the elution time. The amount of Dox in both fractions was measured using the spectrophotometer.

2.4. Analysis of the structure of Dox-MBs fragment species

The structure of fragment species of Dox-MBs was observed using the cryo-EM imaging performed on the FEI Tecnai G2 F20 TWIN TEM (FEI, Hillsboro, OR, USA). Initially, a 200-mesh copper grid-supported holey carbon film (HC200-Cu, Electron Microscopy Sciences, Hatfield, PA, USA) was placed in an argon/oxygen atmosphere and was surface-modified by glow-discharge for 15 s. A 4 μl sample was added onto the copper grid blotted for 3 s in a 100 % humidified chamber at 4 °C. Subsequently, it was flash-frozen in liquid ethane that had been cooled by liquid nitrogen using the Vitrobot sample plunger system (FEI, Hillsboro, OR, USA). The prepared copper grid was stored in liquid nitrogen until imaging. Imaging was conducted in the bright-field mode for cryo-EM with an operating voltage of 200 kV. The images were captured at a magnification of 50,000 × with a 4 k × 4 k charge-coupled device camera (Gatan, Pleasanton, CA, USA).

To investigate the size distribution of fragment species in LDox-MBs and HDox-MBs, the samples with and without US were centrifuged, and the bottom layer solution was analyzed. Particle size and concentration were measured using dynamic light scattering (DLS, model ZetaSizer 3000, Malvern, Worcs., UK). Before analysis, the bottom layer solution was diluted 1000-fold with PBS to achieve concentrations between 10^6 and 10^9 particles/ml.

2.5. Statistics

All data are expressed as means, and standard deviations were measured in at least three independent experiments. Statistical analysis was executed with a two-tailed Student's *t*-test or one-way ANOVA. A p-value less than 0.05 ($p < 0.05$) was considered a significant difference. Correlations were evaluated using Pearson's correlation coefficients. Calculations were executed with the SPSS software package (SPSS Inc., Chicago, IL).

3. Result

3.1. Characteristics of Dox-MBs

We first verify whether the payload would affect the distribution of Dox onto the MB shell by confocal microscopy. A uniform and dense red fluorescence Dox signal was visualized on the shell of MBs in the 500 μg group (LDox-MBs) (Fig. 2A). Several scattered Dox clusters were observed on the outer surface of the MB shell when the dose of Dox was

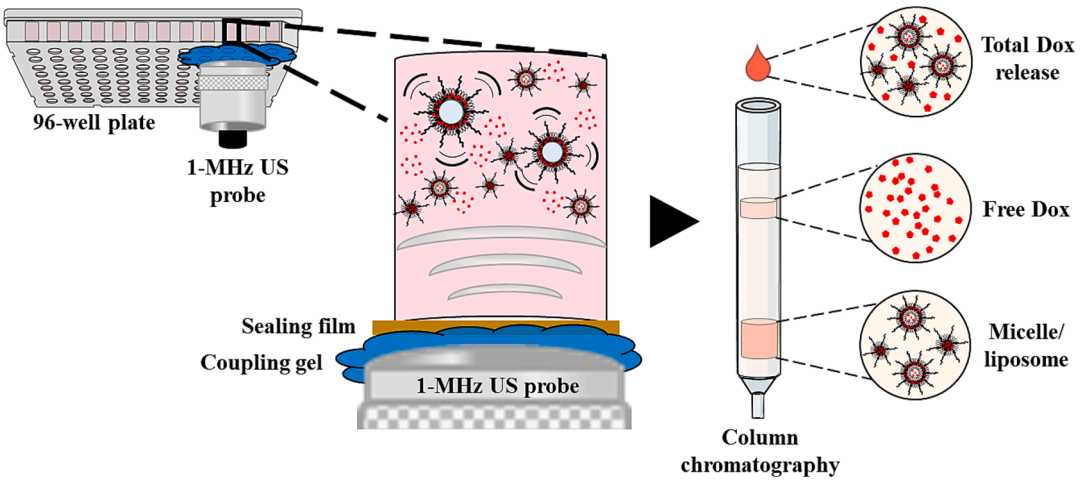

Fig. 1. Setup of column chromatography.

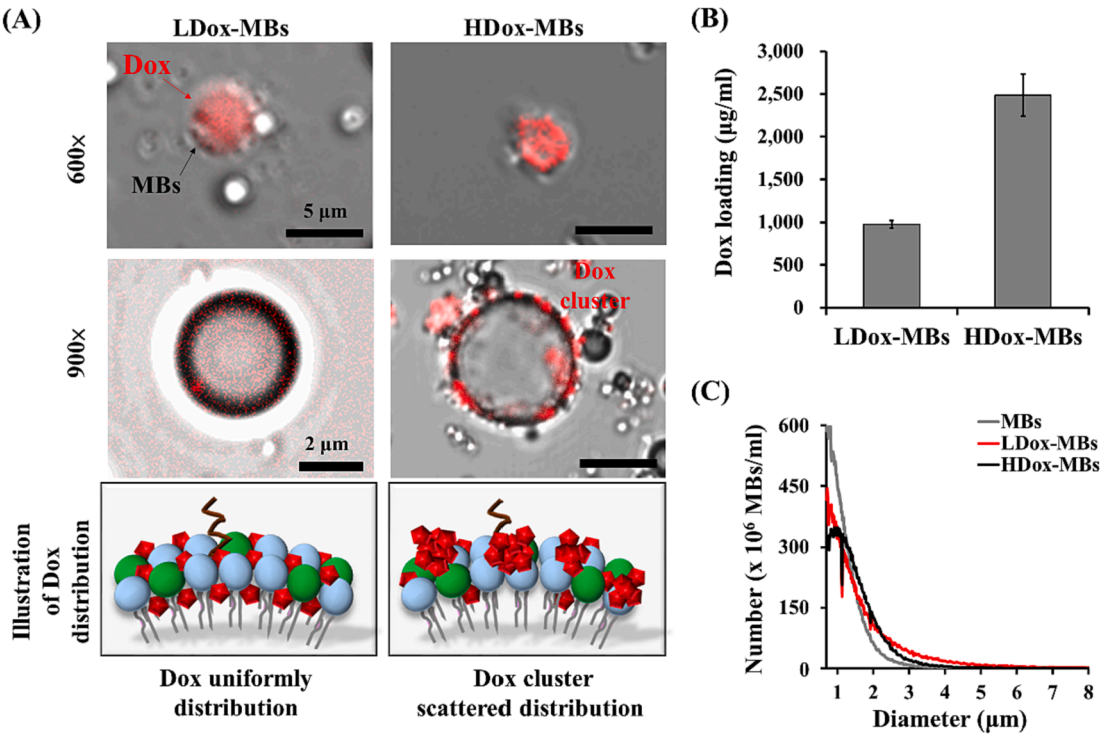

Fig. 2. (A) Dox distribution of L/HDox-MBs. (B) Dox loading. (C) Size distribution. $N = 3$ per group.

increased to 1500 μg (HDox-MBs), which might be attributed to self-aggregation of Dox before attaching to the MBs at such a high concentration [2]. The Dox payload of LDox-MBs and HDox-MBs were 975.0 ± 45.2 μg/ml and 2486.3 ± 245.2 μg/ml (Fig. 2B), respectively, consistent with the microscopic observations. The mean size and concentration of original MBs were 1.0 ± 0.0 μm 37.3 ± 1.3 × 10^9 MBs/ml, respectively. Loading Dox onto MBs resulted in an increase in particle size and a decrease in concentration. Specifically, the particle sizes for LDox-MBs and HDox-MBs were observed to be 1.3 ± 0.0 and 1.3 ± 0.1 μm, respectively, while the concentrations were 28.6 ± 1.6 × 10^9 MBs/ml for LDox-MBs and 27.7 ± 1.7 × 10^9 MBs/ml for HDox-MBs, respectively (Fig. 2C).

The existence of a gas core within the prepared Dox-MBs was then assessed because most US-mediated applications rely on the gaseous substance. The gas core structure of MBs would enhance the contrast of US B-mode imaging. Fig. 3A shows that the two Dox-MBs could provide B-mode imaging contrast enhancement. At 37 °C, the LDox-MBs and HDox-MBs maintained a stability of over 80 % (0 to 60 min, LDox-MBs: 100 ± 0.1 % to 90.7 ± 2.0 %; HDox-MBs: 100 ± 0.1 % to 83.8 ± 7.8 %), probably due to natural gas diffusion from MBs. These data suggest that the prepared Dox-MBs were sufficient for the following experiments.

We next investigated the cavitation activities of these two Dox-MBs with US sonication. The acoustic pressure threshold for stable cavitation of LDox-MBs was 200 kPa. In contrast, no inertial cavitation was detected (Fig. 3B). On the other hand, the acoustic pressure threshold for stable cavitation and inertial cavitation of HDox-MBs were 400 kPa and 400 kPa, respectively (Fig. 3C). Previous had reported that the acoustic properties of MBs were affected by the membrane fluidity of MBs shell [2,20–22]. Also, the membrane fluidity of MBs was reduced by the uniform distribution of Dox on its surface, limiting MBs' vibration range. Therefore, the acoustic pressure threshold for stable and inertial cavitation of HDox-MBs was the same.

3.2. Dox release of Dox-MBs under US sonication

The Dox release of LDox-MBs and HDox-MBs under different parameters of the US was measured in this section. In the LDox-MBs group, the effect of acoustic pressure (0–550 kPa) was first evaluated. The Dox started release when the acoustic pressure exceeded 200 kPa (43319.0 ± 8428.3 and 23630.3 ± 5551.6 a.u. for 0 kPa and 200 kPa) (Fig. 4A), consistent with the pressure threshold of stable cavitation (Fig. 3B). Increasing the acoustic pressure (300–500 kPa) increased Dox release. However, further increasing the pressure to 550 kPa reduced the Dox release (7502.7 ± 7870.5 a.u.). We also noticed two distinct types of substances in the released payload: free Dox and Dox-containing micelle/liposome. The portion of the micelle/liposome in each acoustic pressure maintained 5–7 % (Fig. 4B). We also confirmed that neither increasing the cycle number (100–10000 cycles) nor increasing sonication duration (1–10 min) improved the Dox release (Fig. 4C, 4E). Moreover, the micelle/liposome portion in each acoustic pressure is maintained 5–7 % (Fig. 4D, 4F).

The Dox release of HDox-MBs in response to the US exhibited a different trend. The Dox release began when the acoustic pressure was elevated to 400 kPa (38605.7 ± 1479.4 vs. 22823.3 ± 5614.9 a.u. for 0 kPa and 400 kPa) (Fig. 5A), consistent with the pressure threshold of stable/inertial cavitation (Fig. 3C). The portion of the micelle/liposome was also significantly increased to 8–12 % starting from 400 kPa (Fig. 5B). We also determined the effect of cycle number and found that increasing the cycle number to 10,000 resulted in a significantly enhanced in Dox release compared with 100 group and 1000 group (Fig. 5C). Meanwhile, the portion of the micelle/liposome dropped from 12 % to 7 % (100 to 10000 cycles) (Fig. 5D). In the effect of sonication duration, 10 min group produced a significant increase in Dox release compared with other groups (Fig. 5E), and an obviously drop in the portion of the micelle/liposome (11 % to 5 %, for 10 min and 1 min) (Fig. 5F). The possible reason was that both increasing cycle number and sonication duration would induce more MBs release their payload or destroy the micelle/liposome. Given that the micelle/liposome portion was vastly decreased after US sonication, we speculated that the micelle/liposome might be responsible for the enhanced Dox release.

We then used the DLS and cryo-EM to analyze the size distribution and structure of the released micelle/liposome in different Dox-MBs

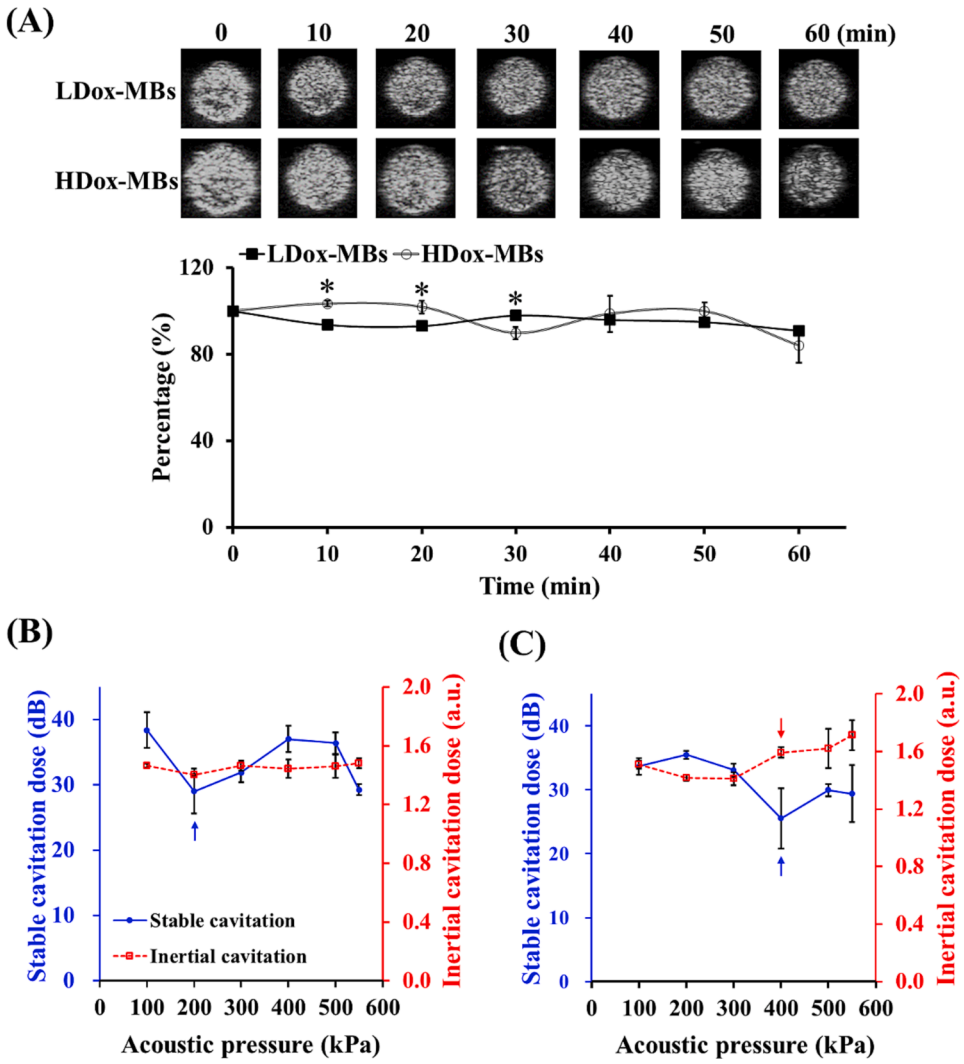

Fig. 3. (A) Acoustic stability of L/HDox-MBs, and stable/inertial cavitation threshold of (B) LDox-MBs and (C) HDox-MBs. Asterisk indicates comparison among LDox-MBs and HDox-MBs. * $p < 0.05$. $N = 3$ per group. Blue arrow: the threshold of stable cavitation; red arrow: the threshold of inertial cavitation.

with different FUS sonication durations. In the LDox-MBs group, the mean size of the micelle/liposome was slightly decreased as the sonication duration increased (282.0 ± 7.9 nm to 268.2 ± 1.9 nm for 0 min to 10 min) (Fig. 6A). However, in HDox-MBs group, the mean size of micelle/liposome at 0 min, 4 min, and 10 min were 412.8 ± 65.3, 330.5 ± 7.0 nm, and 256.1 ± 38.7 nm, respectively (Fig. 6B). The cryo-EM images showed that the released micelle/liposome in LDox-MBs group ranged from 1 to 3 layers at each sonication duration (Fig. 6C). The proportion of 1-layer structure at 0 min and 10 min were 83.0 % and 86.5 %, respectively (Fig. 6D). In the HDox-MBs group, 1–3 layers of micelle/liposome were observed in the 0 min group and 4 min group. Interestingly, we observed 3–5 layers of micelle/liposome in the 10 min group, probably due to the multiple US-induced destruction and self-assembly (Fig. 6C, 6E). These results confirmed that the impact of US with long sonication duration was sufficient to destroy the micelle/liposome and further release to Dox.

4. Discussion

This study aims to answer two questions: (1) the impact of Dox loading on L/HDox-MBs and subsequent payload release, and (2) how acoustic parameters regulate the payload release. Regarding the overall effect of Dox loading, variations in Dox concentrations influenced microscopic imaging outcomes and significantly affected the types of payload released. Specifically, L/HDox-MBs synthesized with 500 and 1500 μg of Dox differed 2.5-fold in drug loading (975.0 ± 45.2 vs 2486.3 ± 245.2 μg/ml). Previously published literature reported the Dox payload of 350–750 μg/ml [23–26], while the Dox payload in our study is approximately three times higher than previous research. Microscopic imaging revealed a uniform, dot-like pattern of Dox on the shell of LDox-MBs. In contrast, HDox-MBs exhibited stronger fluorescence and aggregation (Fig. 2A). Upon analyzing the HDox-MBs drug release pattern in Fig. 5, the short cycle and duration groups showed no significant drug release difference compared to the control. However, a significant difference ($p < 0.05$) emerged with a longer cycle and duration. Notably, micelle/liposome and free Dox release forms were observed in the high Dox release groups. This suggests that HDox-MBs might have a secondary drug release due to fragment species. DLS findings in Fig. 6B confirmed the micelle/liposome formation, aligning with the Fig. 5 results. Cryo-EM revealed that LDox-MBs (uniformly) had a 1-layer cladding structure in over 80 % of fragment species. At the same time, HDox-MBs (cluster) layers increased from 2–3 to 2–5 post-US exposure (Fig. 6C). This implies an increased number of layers in HDox-MBs fragment species post-secondary release.

The cryo-EM showed distinct structural differences in the released nanoparticles from L/HDox-MBs under US sonication. It has reported that when nanocapsules are released via the US, surrounding silica acts as an adhesive, causing the nanocapsules to adhere to each other and

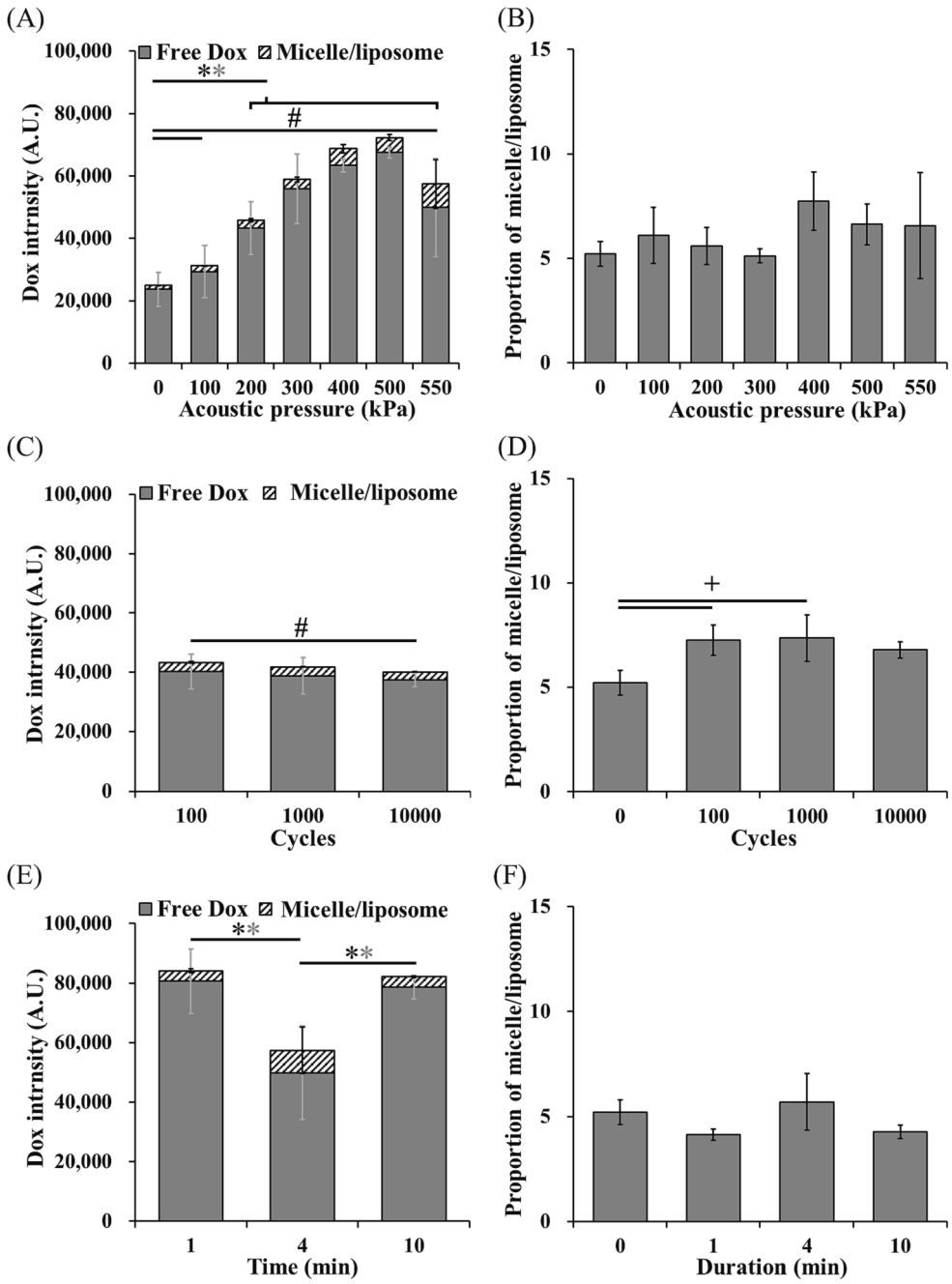

Fig. 4. Total Dox release and the portion of micelle/liposome of LDox-MBs with different US parameters. (A, B) acoustic pressure, (C, D) cycles and (E, F) duration. $N = 3$ per group. Asterisk indicates comparison among total Dox release, grey asterisk indicates comparison among free Dox, and # indicates comparison among micelle/liposome. *, + and # $p < 0.05$.

leading to unique chain-like aggregations in a chain-like manner [27]. In our study, Dox might serve as this adhesive. When exposed to US, a high concentration of released Dox (Fig. 5) caused HDox-MBs to adhere to one another, resulting in multilayered fragment species (Fig. 6C). In contrast, the lower Dox loading in LDox-MBs (Fig. 2B) led to insufficient adhesive forces, generating predominantly cladding structures for the released fragment species (Fig. 6C). In future endeavors to more thoroughly investigate the relationship between various drug-loading amounts and the release of fragment species, this study might draw upon the team's prior research findings and evaluate groups with Dox loadings such as 300 or 3000 μg [2].

Regarding how acoustic parameters influence fragment species' release, we observed that the applied acoustic parameters influenced the payload release and their portion from L/HDox-MBs. The correlation analysis of LDox-MBs revealed that the release of free Dox was significantly influenced by acoustic pressure (R^2 = 0.77) (Fig. S1A). In contrast, the release of micelle/liposome was more impacted by the cycle (R^2 = -0.76) (Fig. S1B). For HDox-MBs, free Dox release was notably affected by duration (R^2 = 0.91) (Fig. S1C), and micelle/liposome release was influenced by acoustic pressure (R^2 = 0.91) (Fig. S1A). Despite the inconsistent performance between LDox-MBs and HDox-MBs in terms of free Dox and micelle/liposome release, an increase in acoustic pressure primarily resulted in free Dox release until approaching the inertial cavitation threshold, where micelle/liposome release became significant (Fig. 3B, 4). Our findings suggest that the critical acoustic parameter affecting fragment species release in Dox-

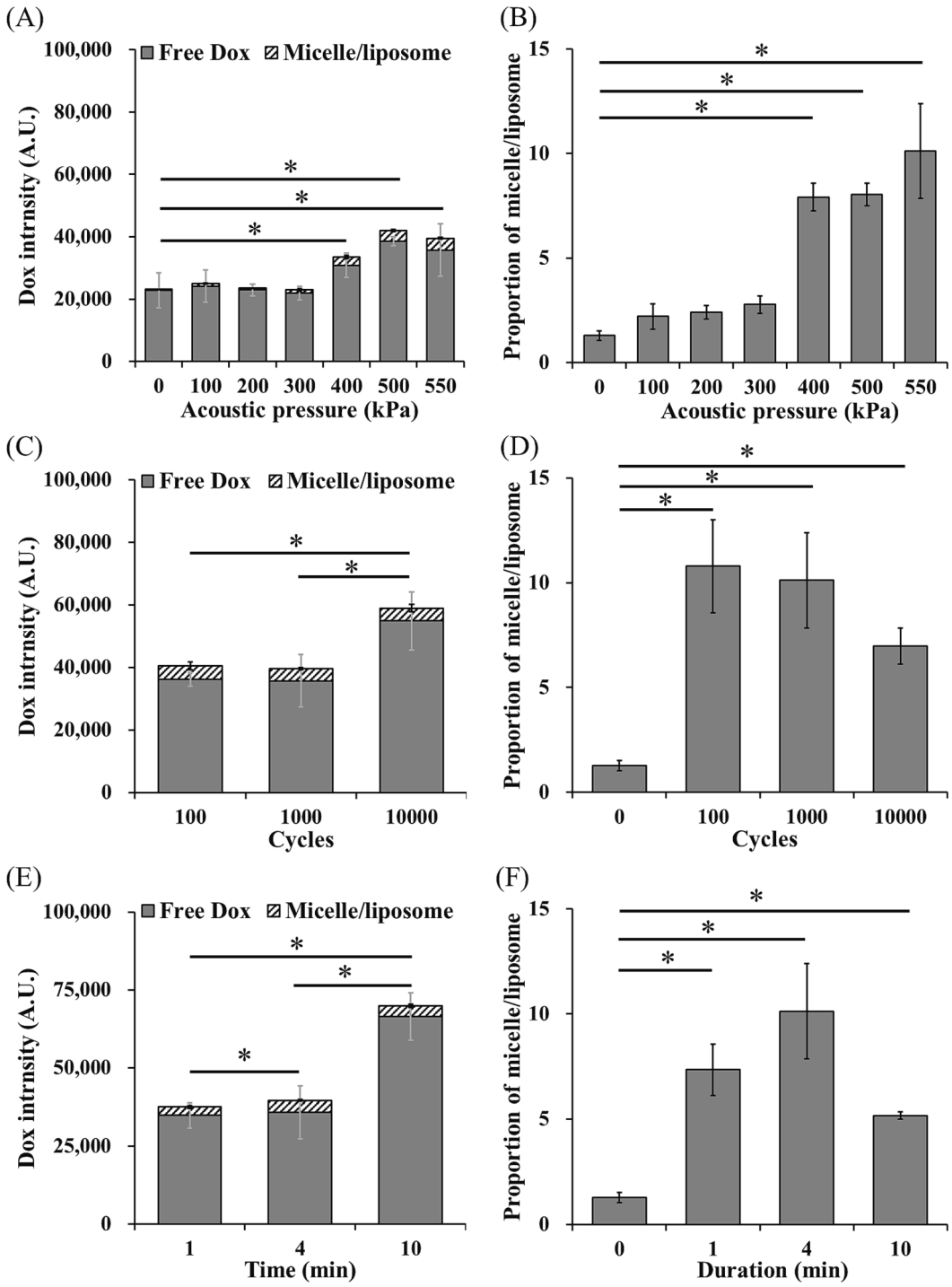

Fig. 5. Total Dox release and the portion of micelle/liposome of HDox-MBs with different US parameters. (A, B) acoustic pressure, (C, D) cycles and (E, F) duration. $N = 3$ per group. Asterisk indicates comparison among total Dox release, grey asterisk indicates comparison among free Dox, and # indicates comparison among micelle/liposome. *, + and # $p < 0.05$.

loaded L/HDox-MBs is acoustic pressure, confirmed by its strong correlation with free Dox and micelle/liposome release in LDox-MBs and HDox-MBs ($R^2 = 0.77$ and 0.91) (Fig. S1, 4, 5).

Although research discussing the impact of acoustic parameters on the release of fragment species from drug-loaded MBs is limited, preliminary observations from existing studies have been noted [4,14,15,28,29]. Common drug-loading strategies in MBs include direct shell loading, and liposome-loaded MBs [4,14,29]. Regarding immediate shell loading, a method closely related to our research, Snipstad et al. incorporated nanoparticles-loaded MBs into cells and observed cellular uptake under-regulated acoustic parameters. They confirmed that the US enhanced cellular uptake depending on acoustic pressure and duty cycle [28]. Ting et al. demonstrated that MBs loaded with 1,3-bis(2-chloroethyl)-1-nitrosourea reached saturation in drug release at 500 kPa (64.66 ± 0.56 %), indicating that higher acoustic pressure did not significantly increase drug release. However, adjusting the pulse repetition frequency to increase the duty cycle could further enhance release (10 Hz, 68.91 ± 3.68 %) [14]. Regarding liposome-loaded MBs, Yu et al. found that 50 % duty cycles were three times more effective than 1500 kPa acoustic pressure in enhancing drug release from liposome-loaded

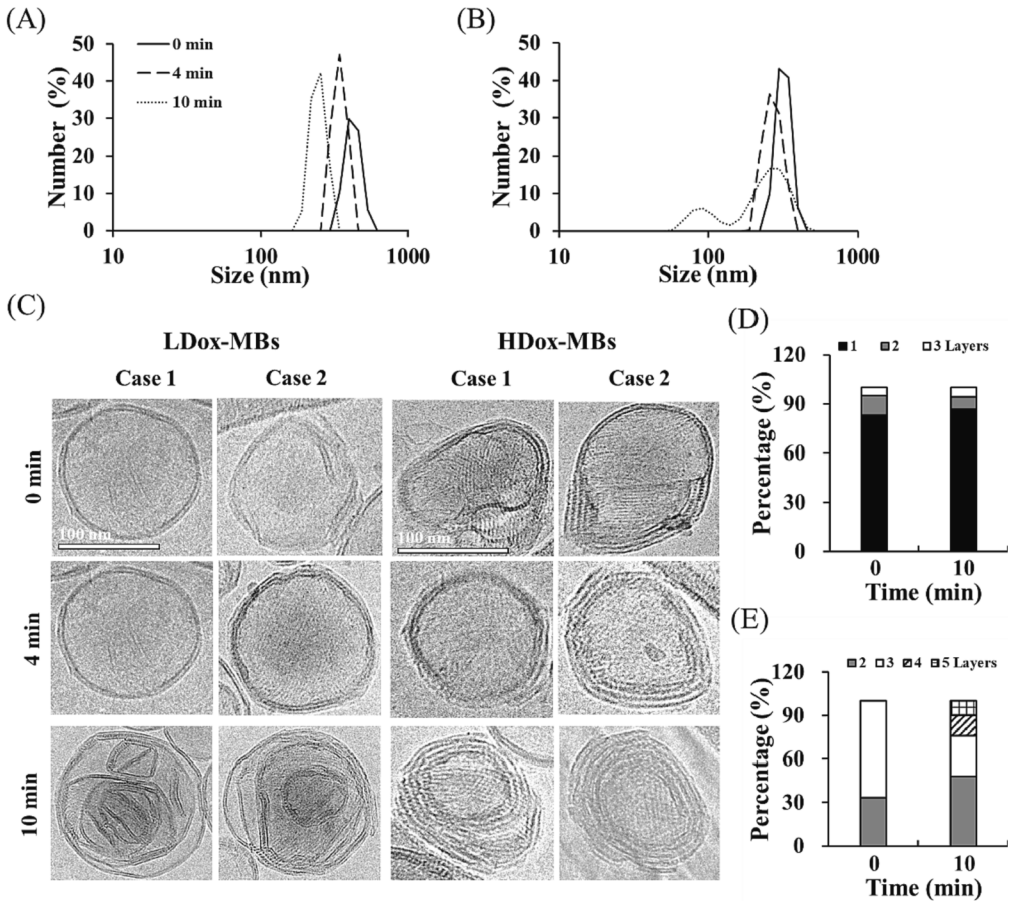

Fig. 6. Size distribution of micelle/liposome before and after US sonication in (A) LDox-MBs and (B) HDox-MBs. (C) The cryo-EM of micelle/liposome before and after US sonication in LDox-MBs and HDox-MBs. (C) The portion of layer number with different sonication duration in LDox-MBs. (D) The portion of layer number with different sonication duration in HDox-MBs.

MBs (67 vs 20 %) [15]. These findings suggest that the critical acoustic parameters affecting drug release appear to be acoustic pressure and duty cycle, similar to our finding.

On the other hand, 33–55 % of total drug release were detected in L/HDox-MBs at 0 kPa, suggesting the Dox leakage from MBs. While such leakage might impact subsequent clinical applications, it's noteworthy that drug leakage can occur across different drug-loaded scenarios. Furthermore, the increased target region permeability induced by the US can enhance drug accumulation. A study by Ueno et al. indicated that the cell membrane's permeability temporarily increases, facilitating significant drug accumulation at tumor sites [30]. In the future, the utilization of lipophilic drugs, such as camptothecin, is anticipated to reduce the occurrence of drug leakage.

5. Conclusion

This study demonstrated that the cavitation activity and the payload release behavior of drug-loaded MBs highly depended on the drug distribution onto the shell of MBs. For uniformly loaded MBs, the drug release could be only triggered by stable cavitation. However, in cluster-loaded MBs, the drug release would be accompanied by stable cavitation and inertial cavitation. We also noticed two distinct substances in the released payload from Dox-MBs: free Dox and micelle/liposome. The portion of the micelle/liposome in each acoustic parameter was maintained at 5–15 %. Furthermore, the micelle/liposome in cluster-loaded MBs has the potential for multiple drug releases upon US sonication. We believe these results will enhance our comprehension of drug-loaded MBs-mediated drug delivery for different therapeutic scenarios. Future work from our team will explore the fragment species formed by diverse drugs and loading techniques. On another front, we will delve deeper into the impact of different fragment species compositions on cellular and animal models. It is envisaged that future advancements in controlling the release of fragment species could achieve objectives of rapid onset and extended duration of therapeutic effects, with implications for clinical applications.

CRediT authorship contribution statement

Chia-Wei Lin: Formal analysis, Investigation, Project administration, Software, Validation, Visualization, Writing – original draft. **Ching-Hsiang Fan:** Visualization, Writing – review & editing. **Chih-Kuang Yeh:** Conceptualization, Funding acquisition, Methodology, Resources, Supervision, Writing – review & editing.

Declaration of competing interest

The authors declare that they have no known competing financial interests or personal relationships that could have appeared to influence the work reported in this paper.

Data availability

The data that has been used is confidential.

Acknowledgments

The authors gratefully acknowledge the support of the National Science and Technology Council (NSTC) of Taiwan under grant nos.

110-2221-E-007-019-MY3, 111-2221-E-007-019-MY3, 112-2321-B-002-021, and 112-2636-E-006-007, by National Tsing Hua University (Hsinchu, Taiwan) under grants no. 112Q2713E1 to C.H.F. and C.K.Y. Moreover, we thank the Academia Sinica Cryo-EM Facility (ASCEM) and Yuan-Chih Chang for their invaluable assistance in cryo-EM imaging.

Appendix A. Supplementary data

Supplementary data to this article can be found online at https://doi.org/10.1016/j.ultsonch.2023.106728.

References

[1] R.A. Barmin, A. Dasgupta, A. Rix, M. Weiler, L. Appold, S. Rutten, F. Padilla, A.J.C. Kuehne, A. Pich, L. De Laporte, F. Kiessling, R.M. Pallares, T. Lammers, Enhanced Stable Cavitation and Nonlinear Acoustic Properties of Poly(butyl cyanoacrylate) Polymeric Microbubbles after Bioconjugation, ACS Biomater Sci Eng, (2022).
[2] C.W. Lin, C.H. Fan, C.K. Yeh, The Impact of Surface Drug Distribution on the Acoustic Behavior of DOX-Loaded Microbubbles, Pharmaceutics 13 (2021).
[3] F. Yan, L. Li, Z. Deng, Q. Jin, J. Chen, W. Yang, C.K. Yeh, J. Wu, R. Shandas, X. Liu, H. Zheng, Paclitaxel-liposome-microbubble complexes as ultrasound-triggered therapeutic drug delivery carriers, J. Control. Release 166 (2013) 246–255.
[4] A. Upadhyay, B. Yagnik, P. Desai, S.V. Dalvi, Microbubble-Mediated Enhanced Delivery of Curcumin to Cervical Cancer Cells, ACS Omega 3 (2018) 12824–12831.
[5] G. Zhao, Q. Huang, F. Wang, X. Zhang, J. Hu, Y. Tan, N. Huang, Z. Wang, Z. Wang, Y. Cheng, Targeted shRNA-loaded liposome complex combined with focused ultrasound for blood brain barrier disruption and suppressing glioma growth, Cancer Lett. 418 (2018) 147–158.
[6] Y.J. Ho, H.C. Chang, C.W. Lin, C.H. Fan, Y.C. Lin, K.C. Wei, C.K. Yeh, Oscillatory behavior of microbubbles impacts efficacy of cellular drug delivery, J. Control. Release 333 (2021) 316–327.
[7] E. Gelderblom, Ultra-high-speed fluorescence imaging, University of Twente, 2012.
[8] Y. Luan, G. Lajoinie, E. Gelderblom, I. Skachkov, A.F. van der Steen, H.J. Vos, M. Versluis, N. De Jong, Lipid shedding from single oscillating microbubbles, Ultrasound Med. Biol. 40 (2014) 1834–1846.
[9] J.R. Eisenbrey, M.C. Soulen, M.A. Wheatley, Delivery of encapsulated Doxorubicin by ultrasound-mediated size reduction of drug-loaded polymer contrast agents, I.E. E.E. Trans. Biomed. Eng. 57 (2010) 24–28.
[10] S. Roovers, G. Lajoinie, I. De Cock, T. Brans, H. Dewitte, K. Braeckmans, M. Versuis, S.C. De Smedt, I. Lentacker, Sonoprinting of nanoparticle-loaded microbubbles: Unraveling the multi-timescale mechanism, Biomaterials 217 (2019), 119250.
[11] D. Ingato, J.A. Edson, M. Zakharian, Y.J. Kwon, Cancer Cell-Derived, Drug-Loaded Nanovesicles Induced by Sulfhydryl-Blocking for Effective and Safe Cancer Therapy, ACS Nano 12 (2018) 9568–9577.
[12] A. Gabizon, H. Shmeeda, Y. Barenholz, Pharmacokinetics of pegylated liposomal Doxorubicin: review of animal and human studies, Clin. Pharmacokinet. 42 (2003) 419–436.
[13] P.K. Working, M.S. Newman, S.K. Huang, E. Mayhew, J. Vaage, D.D. Lasic, Pharmacokinetics, Biodistribution and Therapeutic Efficacy of Doxorubicin Encapsulated in Stealth® Liposomes (Doxil®), J. Liposome Res. 4 (2008) 667–687.
[14] C.Y. Ting, C.H. Fan, H.L. Liu, C.Y. Huang, H.Y. Hsieh, T.C. Yen, K.C. Wei, C.K. Yeh, Concurrent blood-brain barrier opening and local drug delivery using drug-carrying microbubbles and focused ultrasound for brain glioma treatment, Biomaterials 33 (2012) 704–712.
[15] F.T. Yu, X. Chen, J. Wang, B. Qin, F.S. Villanueva, Low Intensity Ultrasound Mediated Liposomal Doxorubicin Delivery Using Polymer Microbubbles, Mol. Pharm. 13 (2016) 55–64.
[16] S. Tinkov, G. Winter, C. Coester, R. Bekeredjian, New doxorubicin-loaded phospholipid microbubbles for targeted tumor therapy: Part I-Formulation development and in-vitro characterization, J. Control Release 143 (2010) 143–150.
[17] K. Cheung, O. Couture, P.D. Bevan, E. Cherin, R. Williams, P.N. Burns, F.S. Foster, In vitro characterization of the subharmonic ultrasound signal from Definity microbubbles at high frequencies, Phys. Med. Biol. 53 (2008) 1209–1223.
[18] S.T. Kang, J.L. Lin, C.H. Wang, Y.C. Chang, C.K. Yeh, Internal polymer scaffolding in lipid-coated microbubbles for control of inertial cavitation in ultrasound theranostics, J. Mater. Chem. B 3 (2015) 5938–5941.
[19] C.H. Fan, E.L. Chang, C.Y. Ting, Y.C. Lin, E.C. Liao, C.Y. Huang, Y.C. Chang, H. L. Chan, K.C. Wei, C.K. Yeh, Folate-conjugated gene-carrying microbubbles with focused ultrasound for concurrent blood-brain barrier opening and local gene delivery, Biomaterials 106 (2016) 46–57.
[20] E.L. Chang, C.Y. Ting, P.H. Hsu, Y.C. Lin, E.C. Liao, C.Y. Huang, Y.C. Chang, H. L. Chan, C.S. Chiang, H.L. Liu, K.C. Wei, C.H. Fan, C.K. Yeh, Angiogenesis-targeting microbubbles combined with ultrasound-mediated gene therapy in brain tumors, J. Control. Release 255 (2017) 164–175.
[21] Y. Gu, C. Chen, J. Tu, X. Guo, H. Wu, D. Zhang, Harmonic responses and cavitation activity of encapsulated microbubbles coupled with magnetic nanoparticles, Ultrason. Sonochem. 29 (2016) 309–316.
[22] C.Y. Wu, R.Y. Huang, E.C. Liao, Y.C. Lin, Y.J. Ho, C.W. Chang, H.L. Chan, Y. Z. Huang, T.H. Hsieh, C.H. Fan, C.K. Yeh, A preliminary study of Parkinson's gene therapy via sono-magnetic sensing gene vector for conquering extra/intracellular barriers in mice, Brain Stimul. 13 (2020) 786–799.
[23] S. Tinkov, C. Coester, S. Serba, N.A. Geis, H.A. Katus, G. Winter, R. Bekeredjian, New doxorubicin-loaded phospholipid microbubbles for targeted tumor therapy: in-vivo characterization, J. Control. Release 148 (2010) 368–372.
[24] R. Abdalkader, S. Kawakami, J. Unga, R. Suzuki, K. Maruyama, F. Yamashita, M. Hashida, Evaluation of the potential of doxorubicin loaded microbubbles as a theranostic modality using a murine tumor model, Acta Biomater. 19 (2015) 112–118.
[25] C.H. Fan, C.Y. Ting, H.J. Lin, C.H. Wang, H.L. Liu, T.C. Yen, C.K. Yeh, SPIO-conjugated, doxorubicin-loaded microbubbles for concurrent MRI and focused-ultrasound enhanced brain-tumor drug delivery, Biomaterials 34 (2013) 3706–3715.
[26] Z. Gao, A.M. Kennedy, D.A. Christensen, N.Y. Rapoport, Drug-loaded nano/microbubbles for combining ultrasonography and targeted chemotherapy, Ultrasonics 48 (2008) 260–270.
[27] Y. Steinberg, A. Schroeder, Y. Talmon, J. Schmidt, R.L. Khalfin, Y. Cohen, J. M. Devoisselle, S. Begu, D. Avnir, Triggered release of aqueous content from liposome-derived sol-gel nanocapsules, Langmuir 23 (2007) 12024–12031.
[28] S. Snipstad, S. Hanstad, A. Bjorkoy, Y. Morch, C. de Lange Davies, Sonoporation Using Nanoparticle-Loaded Microbubbles Increases Cellular Uptake of Nanoparticles Compared to Co-Incubation of Nanoparticles and Microbubbles, Pharmaceutics 13 (2021).
[29] J.M. Escoffre, C. Mannaris, B. Geers, A. Novell, I. Lentacker, M. Averkiou, A. Bouakaz, Doxorubicin liposome-loaded microbubbles for contrast imaging and ultrasound-triggered drug delivery, IEEE Trans. Ultrason. Ferroelectr. Freq. Control 60 (2013) 78–87.
[30] Y. Ueno, S. Sonoda, R. Suzuki, M. Yokouchi, Y. Kawasoe, K. Tachibana, K. Maruyama, T. Sakamoto, S. Komiya, Combination of ultrasound and bubble liposome enhance the effect of doxorubicin and inhibit murine osteosarcoma growth, Cancer Biol. Ther. 12 (2011) 270–277.